Theoret. Comput. Fluid Dynamics (2000) 13: 397–419

Theoretical and Computational Fluid Dynamics

Response of the Sphere Wake to Freestream Fluctuations

R. Mittal

Department of Mechanical Engineering, University of Florida,
Gainesville, FL 32611, U.S.A.

Communicated by M.Y. Hussaini

Received 5 October 1999 and accepted 14 October 1999

Abstract. Direct numerical simulations have been used to investigate the response of the wake of a sphere to freestream fluctuations. This study has been motivated by the need to understand particle-induced turbulence enhancement in particulate flows. A sequence of simulations of flow past a sphere have been carried out where the frequency and amplitude of the freestream fluctuations and the flow Reynolds number has been varied systematically. It has been suggested that turbulence enhancement is primarily caused by vortex shedding from particles (Gore and Crowe, 1989; Hetsroni, 1989). Our simulations of the forced wake indicate that turbulence enhancement may be attributed to natural vortex shedding only when the freestream fluctuation level is low and the Reynolds number is greater than about 300. In addition to natural vortex shedding, the current simulations also suggest another mechanism for turbulence enhancement. It is found that in the presence of freestream fluctuations, the wake behaves like an oscillator and returns large amounts of kinetic energy to the surrounding fluid at resonance. This mechanism is not associated with natural vortex shedding and is therefore capable of enhancing freestream turbulence even at Reynolds numbers less than 300. Simulations also indicate that when the turbulence intensity of the carrier fluid is high, this resonance mechanism might be solely responsible for turbulence enhancement. Finally, our simulations also suggest a possible explanation for the correlation between turbulence enhancement and the ratio of the particle size to the size of energy containing eddies of turbulence found by Gore and Crowe (1989).

1. Introduction

Particulate flows abound in nature as well as in engineering applications and in most cases the flow in question is turbulent. It has been known for some time now that depending on the particular flow configuration, the addition of particles can either reduce or enhance the turbulence level in the carrier phase. Understanding this effect of the particles on the turbulence of the carrier phase is extremely important since in many particulate flows of interest, turbulence can have a significant effect on the transport of mass, momentum, energy, and species and for a particular application this effect may be desirable or undesirable. This has been the motivation for a large number of studies on particle–turbulence interaction that have been carried out to date.

One of the earliest attempt at understanding the various aspects of gas-particle flows was made by Owen (1969). He postulated that the particle Stokes number was the key parameter that controlled particle–turbulence interaction. The particle Stokes number, S, is defined as the ratio of the particle aerodynamic response time to the characteristic time scale of the energy-containing motion (or eddy turnover time). For $S \ll 1$, he argued that the rapid response of the particles to the eddy motion would extract energy out of the turbulence which would subsequently be dissipated, thereby leading to a reduction in the turbulent intensity. For $S \gtrsim 1$, he argued that the particles would respond partially to the turbulent motions and still be able

to extract and dissipate some turbulent energy. Finally, for $S \gg 1$ he suggested that the particles could be considered as fixed in space and their effect on turbulence would be distortional, similar to the effect of a gauze screen.

Hetsroni (1989) has postulated that the enhancement of turbulence is due to vortex shedding from particles and that the particle Reynolds number ($Re_\mathrm{p} = u_\mathrm{r} d/v$ where u_r is the velocity of particle relative to the surrounding fluid and d is the diameter of the particle) primarily determines the degree to which turbulence is enhanced. However, in experiments it is difficult to estimate the particle Reynolds number, much less observe vortex shedding from the particles and therefore only indirect support for this postulate could be provided. Based mainly on the data from the experiments of Tsuji and coworkers (1982, 1984, 1988), Hetsroni concluded that particles with $Re_\mathrm{p} < 100$ suppressed turbulence whereas particles with $Re_\mathrm{p} > 400$ enhanced it. In the intermediate range, not enough data was available and the effect on turbulence was mixed. Based on the fact that Achenbach (1974) had reported that natural vortex shedding from a sphere immersed in a steady, uniform stream (referred to in this paper as natural vortex shedding) starts at a Reynolds number ($Re_d = U_\infty d/v$ where U_∞ is the freestream velocity) of about 400, Hetsroni concluded that turbulence enhancement was due to vortex shedding from particles. However, other investigations have shown that vortex shedding in the sphere wake is initiated at Reynolds numbers as low as 290 (Margavey and Bishop, 1961; Natarajan and Acrivos, 1993). Furthermore, it is also not clear to what extent natural vortex shedding is affected by freestream fluctuations. In an experimental investigation Wu and Faeth (1994) found that low intensity ($\lesssim$ 4% turbulence intensity) freestream turbulence does not alter the vortex shedding process in any significant manner. The effect of higher intensity turbulence on natural vortex shedding is however not known. Recent simulations by Yusof (1996) have shown that in the presence of higher intensity ($>$ 12%) freestream turbulence the wake of a sphere can become unstable at Reynolds numbers as low as 100 which indicates that natural vortex shedding might not be the only mechanism for turbulence enhancement

An explanation of the effect of particles on turbulence has also been provided by Gore and Crowe (1989) who compiled data from numerous experiments on multiphase flows. They plotted the relative increase in turbulence intensity versus the particle-to-eddy size ratio γ_d ($\gamma_d = d_\mathrm{p}/l_\mathrm{e}$ where d_p is the diameter of the particle and l_e is the characteristic size of the energy containing eddies in the turbulent fluid) and made the interesting observation that turbulence was enhanced only when $\gamma_d \gtrsim 0.1$. Data extracted from this plot is reproduced in Figure 1. The explanation put forth by Gore and Crowe to explain the observed trend was that dispersion of small particles extracts energy out of the fluid turbulence whereas fluctuations created by vortex shedding in the wake of large particles adds to the energy of turbulence. However, no explanation was provided regarding the particular value of γ_d where this transition from turbulence suppression to turbulence enhancement took place.

Recently Pan and Bannerjee (1997) have investigated the effect of large particles on wall-bounded turbulence through numerical simulations. In their simulations, a finite number of large particles have been included in the flow with the particles modeled through a momentum forcing technique. The study indicates that small particles tend to suppress turbulence by diminishing sweep events whereas larger particles have exactly the opposite effect. This is an extremely interesting and useful finding since it directly connects the effect of particles to an important mechanism of turbulence production. Furthermore, this study also clearly demonstrates how additional insight into particle-induced turbulence modulation can be gained by including finite particle size effects in numerical simulations. However, this study does not address the interaction of particles with turbulence away from the wall. Furthermore, no attempt has been made in this study to connect turbulence enhancement with vortex shedding from particles.

In summary, even though the explanations of Hetsroni (1989) and Gore and Crowe (1989) seem plausible, there is no direct evidence to support the argument that vortex shedding from particles is indeed a factor in particle-induced turbulence enhancement since vortex shedding from particles in a turbulent flow has not been observed in experiments or in simulations. Furthermore, a clear understanding of the physical mechanism that leads to transition from turbulence suppression to enhancement at a particle-to-eddy size ratio of about 0.1 is also not forthcoming. Addition of energy to the carrier phase due to vortex shedding as suggested by Hetsroni and Gore and Crowe is one possibility. There are, however, other mechanisms related to the finite size of the particle that might play a role in particle–turbulence interaction. There is the possibility that the particle-to-eddy size ratio might itself be an important parameter and the underlying physical mechanism connected with the direct interaction of energy-containing turbulent eddies and wake vortices of similar length scales.

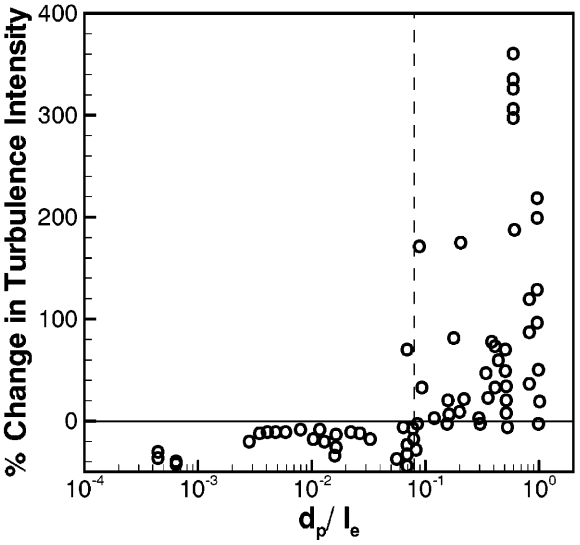

Figure 1. Percentage change in turbulence intensity versus particle-to-eddy size ratio. The data in this plot have been extracted from the paper of Gore and Crowe (1989). The vertical dashed line indicates the particle-to-eddy size ratio above which turbulent is enhanced by the particles.

Since vortex shedding from particles is hypothesized to be the key mechanism responsible for turbulence enhancement, it is appropriate to review briefly the current state of knowledge regarding vortex shedding from spheres immersed in a uniform, steady flow. Margavey and Bishop (1961) carried out the first comprehensive experimental study of the low Reynolds number sphere wake and categorized the various regimes that were observed. According to their experiments, the sphere wake is steady and axisymmetric below a Reynolds number of about 200. Beyond Re_d = 200, the wake becomes nonaxisymmetric and dye visualizations exhibit the peculiar "double-thread" type signature. This regime has also been studied in detail by Nakamura (1976) and recent calculations by Natarajan and Acrivos (1993) also indicate a bifurcation to this state at about Re_d = 210. The stability calculations show that this is a regular bifurcation with k_φ = 1 as the most unstable azimuthal mode (see Figure 3).

The double-thread wake remains steady up to a Reynolds numbers of about 277 where it first becomes susceptible to unsteady disturbances (Natarajan and Acrivos, 1993). The stability calculations suggest that k_φ = 1 is again the mode that is most unstable during this Hopf bifurcation. Vortex shedding in the sphere wake has been observed to appear at a Reynolds number of about 290 and is characterized by the formation of streamwise-oriented vortex loops that are shed periodically in the near wake (Margavey and Bishop, 1961; Margavey and MacLatchy, 1965; Sakamoto and Haniu, 1995). The vortex shedding process at these Reynolds numbers is peculiar in that the unsteady wake seems to exhibit a planar symmetry. This has been observed in the experiments of Sakamoto and Haniu (1995) who have indicated that this planar symmetric regime extends up to Re_d = 420. A detailed DNS study of this regime has recently been carried out using the current solver (Mittal, 1999b) and this study indicates that planar symmetry is lost as early as Re_d = 375. Once planar symmetry is lost, the vortex shedding process becomes extremely complicated with vortex loops forming at different azimuthal locations in each shedding cycle. Furthermore, as the Reynolds number is increased to about 500, the vortex loops close in on themselves as they convect downstream and form compact vortex rings. This phenomena has been observed in experiments (Margavey and Bishop, 1961) as well as in direct numerical simulations (Mittal, 1999a).

Sakamoto and Haniu (1990, 1995) have systematically measured the vortex shedding Strouhal number for a large range of Reynolds numbers and data extracted from their plot is presented in Figure 2. The Strouhal number is defined as $St = fd/U_\infty$ where f is the shedding frequency. We have limited this plot to the lower range of Reynolds numbers ($Re_d < 3000$) which is of relevance to particulate flows. The curve marked "low mode" corresponds to the shedding of large-scale vortex loops in the near wake and the Strouhal number for this mode extends from about 0.15 to 0.20 over the range of interest. Measurements of Ormieres and Provensal (1998) and Margavey and Bishop (1961) have also been plotted and these indicate a noticeable

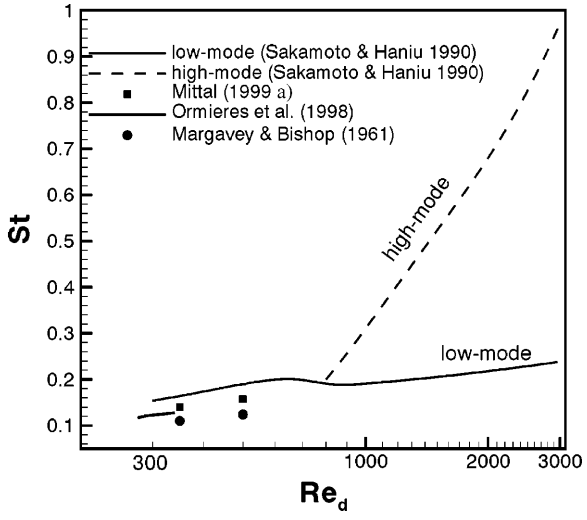

Figure 2. Variation of Strouhal number with Reynolds number for the wake of a sphere. The thin solid and dashed curves denotes the Strouhal number corresponding to the low mode and high mode, respectively, measured by Sakamoto and Haniu (1990). Strouhal numbers obtained from other experiments and our numerical simulations have also been plotted.

spread in the measured Strouhal number at low Reynolds numbers. The lowest measured Strouhal numbers has a value of about 0.1. Strouhal numbers obtained from our simulations (Mittal, 1999a) have also been plotted and these lie between the measured values. In addition to the low mode, there is also the so-called "high mode" which appears at a Reynolds number of about 800. This mode is associated with the formation of small scale Kelvin–Helmholtz vortices in the separated shear layers similar to the Bloor–Gerrard vortices observed in cylinder wakes (Bloor, 1964). Unlike the low mode, the shedding frequency of the high mode increases rapidly with Reynolds number and the Strouhal number of this mode varies from 0.2 to about 1.0 in the range of interest.

Most studies indicate that turbulence enhancement by particles is a consequence of the interaction between individual particles and the turbulent flow and that particle–particle interaction does not play a significant role in this phenomenon. It therefore stands to reason that some of the underlying physical mechanisms can be understood by studying the interaction of a single particle with a turbulent flow. A number of studies have therefore been performed where the objective has been to understand the interaction between a spherical particle and a turbulent or unsteady flow (Wu and Faeth, 1995; Yusof, 1996; Kim *et al.*, 1997a,b). A similar viewpoint is adopted in the current study in that here too we have studied flow past a single, stationary spherical particle. In addition to this, we simplify the situation further by replacing the turbulent flow with a sinusoidally oscillating freestream. Thus, the flow studied here consists of a sphere immersed in a freestream where the cross-flow (transverse) component of velocity is oscillated sinusoidally. We believe that this approach simplifies the flow configuration while retaining some of the relevant flow physics. It is expected that a comprehensive analysis of this simpler flow configuration using direct numerical simulations will help us identify mechanisms responsible for particle-induced turbulence enhancement. It should be pointed out that even this simplified flow configuration has a large multidimensional parameter space which is indicative of the complexity of this problem. The key parameters in this flow are the frequency and amplitude of the freestream fluctuation and the flow Reynolds number. In the current study we have performed a sequence of simulations with the objective of understanding the behavior of the forced sphere wake over a wide range of these parameters.

2. Computational Methodology

A solver based on a Fourier–Chebyshev spectral collocation (Canuto *et al.*, 1988) has been developed for direct numerical simulation of three-dimensional, viscous, incompressible flow past a prolate spheroid. Flow

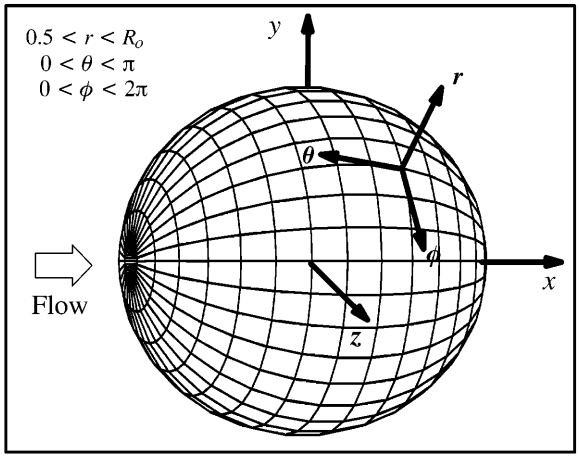

Figure 3. Surface mesh used in the current simulation. The Cartesian as well as the spherical coordinate systems are shown.

past a sphere can be solved as a special case. Here we present only a brief outline of the solver used for the current simulations. For a detailed description the reader is referred to Mittal (1999a).

The governing equations are the unsteady, incompressible Navier–Stokes equations given by continuity

$$\nabla \cdot \boldsymbol{u} = 0, \tag{1}$$

momentum conservation

$$\frac{\partial \boldsymbol{u}}{\partial t} + \boldsymbol{u} \cdot \nabla \boldsymbol{u} = -\nabla P + \frac{1}{Re_d} \nabla^2 \boldsymbol{u}, \tag{2}$$

where $\boldsymbol{u}$ and P are the velocity and pressure, respectively. Furthermore, in the above equations Re_d is the Reynolds number based on the freestream velocity (U_∞) and diameter (d) of the sphere. The above equations are transformed to the prolate spheroidal coordinate system and discretized on an orthogonal curvilinear body-fitted grid. The surface grid for our sphere simulations is shown in Figure 3. The azimuthal direction φ is periodic over 2π and this allows us to use a Fourier collocation method in this direction. In the θ-direction, which is referred to as the wall-tangential direction, the flow is periodic not over π but over 2π, and a restricted Fourier series is used for computing derivatives along this direction. The singularity in the coordinate transformation at the poles which are located at $\theta = 0$ and π has been avoided by distributing the collocation points in such a manner as to avoid these locations. The algorithm also allows us to cluster points in the wake in the θ direction. The semi-infinite flow domain is truncated to a large but finite distance and a Chebyshev collocation method is used in this nonperiodic direction. Thus, spectral discretization is used in all three directions and this results in a highly accurate computation of the derivatives. A typical mesh used in the current simulations contains 121 points in the radial direction and 80 points in the θ direction. In the azimuthal direction, the number of points range from 24 for low Reynolds number to 32 for the higher Reynolds number simulations. Furthermore, the outer boundary of the domain extends to $20d$ for all our simulations. Figure 4 shows a typical mesh used in our simulations. Previous simulations (Mittal, 1999a,b) in this Reynolds number regime have guided us in the choice of the grid and the domain size. Fourier spectra of the flow variables is monitored in both the θ and φ directions and at least five orders of magnitude decay in the energy is ensured. In addition, to show conclusively that 24 azimuthal points are adequate for the low Reynolds number forced wake simulations, we have carried out one such simulation with 32 azimuthal points. A comparison of the results on the two meshes shows no significant differences, thereby confirming the adequacy of the azimuthal resolution.

A two-step time-split scheme (Chorin, 1968) is used for advancing the solution in time. The intermediate velocity field is obtained first by advancing through the advection–diffusion equation; and a second-order accurate, semi-implicit method is used for this step. The radial and azimuthal viscous terms are discretized in an implicit manner using a Crank–Nicolson scheme. All other terms such as the nonlinear convection and other cross-terms that result from the curvilinear nature of the coordinate system are treated explicitly using a second-order Adams–Bashforth scheme. The next step is pressure correction and this requires the

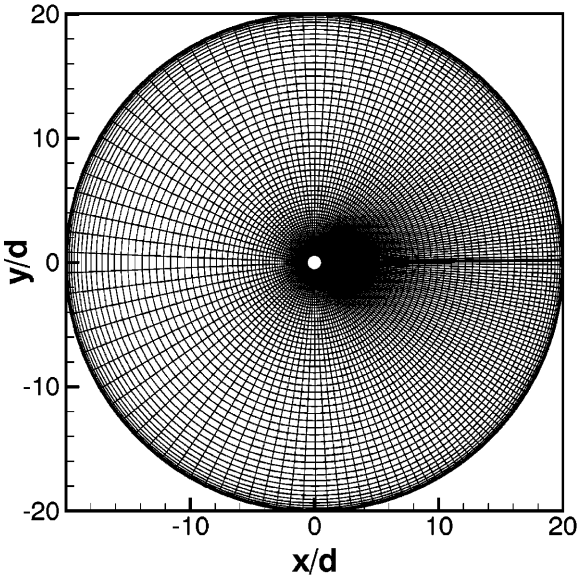

Figure 4. Typical grid used in the current simulation. Note that only a two-dimensional projection of the grid is shown. The three-dimensional grid is obtained by rotating this mesh about the x-axis.

solution of the pressure Poisson equation which is solved with a homogeneous Neumann condition on the boundaries. Finally, the pressure correction is added to the intermediate velocity and a divergence-free velocity field is obtained. A higher-order intermediate velocity boundary condition is used which results in accurate imposition of the no-slip, no-penetration condition on the body. Details of the time-split scheme can be found in Mittal and Balachandar (1996) and Mittal (1999a).

Since the flow domain is truncated to a finite extent in the current simulations, appropriate boundary conditions are required at the outer boundary. Inviscid flow past the spheroid is computed first and this is used as the inflow boundary condition as well as the initial condition. At the outflow boundary we use a previously developed nonreflective boundary condition which allows vortical disturbances to exit the computational domain in a smooth manner without any significant reflections. This boundary treatment has been tested extensively in cylindrical and spheroidal geometries and details of these tests can be found in Mittal and Balachandar (1996) and Mittal (1999a).

3. Results

3.1. Sphere in a Steady Uniform Flow

The current study focuses on the $100 < Re_d < 350$ regime and before we investigate the response of the sphere wake to freestream fluctuations it is insightful to elucidate, through flow visualizations, the topology of the wake and the dynamics of natural vortex shedding when the sphere is immersed in a uniform, steady flow. Here we have chosen to focus on two Reynolds numbers: Re_d = 150 and 350 which represent steady and unsteady wake regimes, respectively. In these two simulations, a small nonaxisymmetric velocity perturbation is provided for a short time duration on the sphere surface at the beginning of the simulation. For Reynolds numbers lower than 210, this perturbation is not amplified and the flow eventually returns to an axisymmetric state. However, at higher Reynolds numbers, this perturbation is amplified by the inherent instability of the wake, and depending on the Reynolds number, either leads to a steady, nonaxisymmetric state or to vortex shedding. Each simulation is continued until a stationary state is obtained and this can take up to 300 nondimensional time units (d/U_∞). Statistics are then accumulated over a time interval of about $300d/U_\infty$.

At Re_d = 150 the wake is axisymmetric and steady and Figure 5 show the streamline pattern and azimuthal vorticity (ω_φ) contours on one r–θ plane of the domain. The flow looks similar to what one would observe

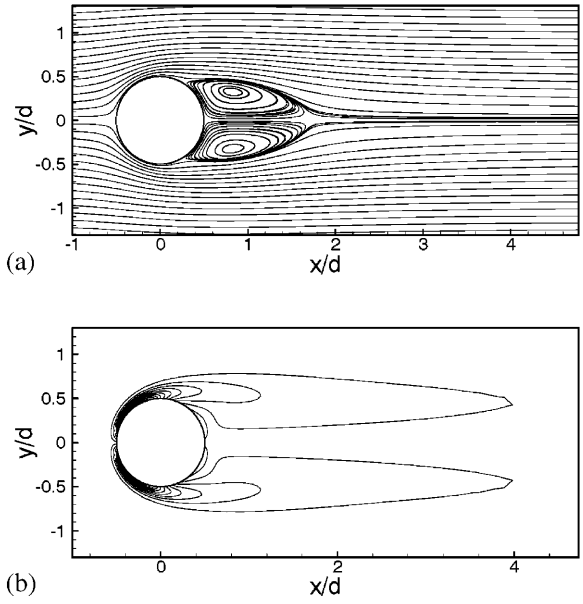

Figure 5. (a) Streamline plot of the axisymmetric flow obtained at Re_d = 150 on one azimuthal plane. (b) Corresponding contour plot of azimuthal vorticity ω_φ.

in the steady wake of a circular cylinder. At Re_d = 350, however, the wake exhibits vortex shedding and Figure 6 shows two views of the vortex topology observed for this flow at one time instant. In our previous studies (Mittal and Balachandar, 1995a), complex three-dimensional vortical structures in cylinder wakes have been identified successfully by the imaginary part of the eigenvalue of the velocity gradient tensor (denoted by $\lambda_{\rm i}$) and we use the same method here for extracting the vortical structures in the sphere wake. Thus, throughout this paper vortical structures in the sphere wake have been visualized by plotting one isosurface of $\lambda_{\rm i}$. The particular value of $\lambda_{\rm i}$ is chosen so as to bring out the most salient features of the vortex topology. For the sphere wake, we have found that $\lambda_{\rm i}$ = 0.1 captures all the important features of the topology and this value has been used for all the flow visualizations presented in this paper.

The most striking feature observed in the bottom view of Figure 6 is the apparent symmetry of the wake about a plane passing through the wake centerline. Change in the orientation of the plane of symmetry can be detected by computing the phase angle between the two component of side force on the sphere. For this

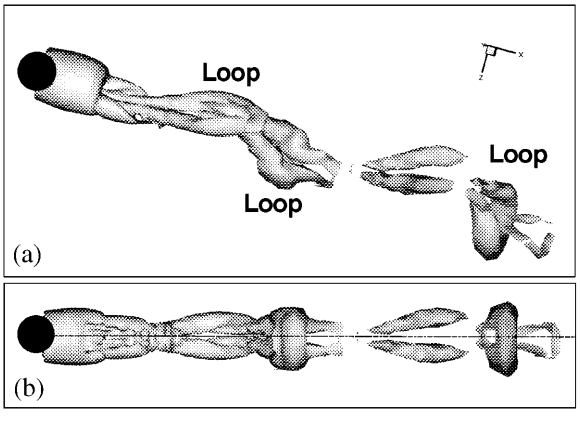

Figure 6. Two views of the vortex topology observed in the wake of a sphere at Re_d = 350. The vortical structures have been visualized by plotting one isosurface of $\lambda_{\rm i}$ corresponding to a value of 0.1. (a) Perspective view of the wake which shows the interconnected loop structure of the vortices. (b) View along the plane of symmetry. The symmetry plane is indicated by a dash-dot line. The isosurface has been terminated near the sphere surface so as to show the position of the sphere clearly.

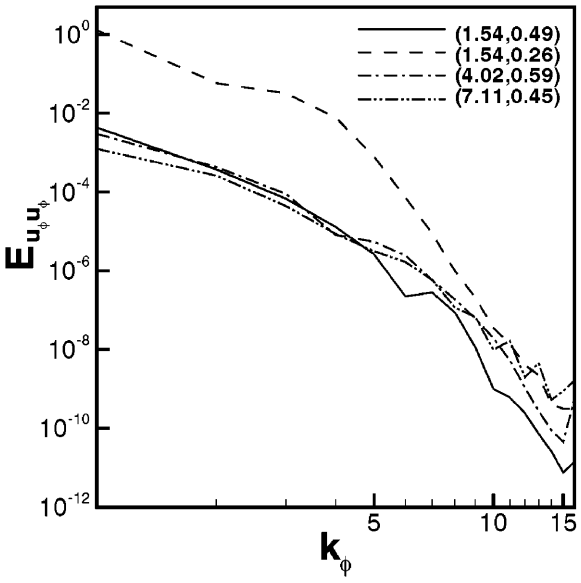

Figure 7. Time averaged azimuthal spectra of the azimuthal velocity component at four locations in the sphere wake. The coordinates of the four locations are shown in the legend.

flow it has been shown (Mittal, 1999b) that the two components are virtually phase locked with negligible change in the phase angle, thereby indicating that the flow in the near wake maintains a fixed plane of symmetry at all times during the shedding process. Furthermore, the top figure shows that vortex shedding is characterized by the appearance of interconnected vortex loops similar in shape to those observed in the experiments (Margavey and Bishop, 1961; Ormieres and Provensal, 1998). The Strouhal number has been computed from the time variation of the azimuthal component of velocity in the near wake and is found to be about 0.14. As mentioned earlier, the spectra of flow quantities is monitored in order to check for the adequacy of the grid resolution. In Figure 7 we have plotted the energy spectra of the azimuthal velocity component in the wake at four different locations. The spectra have been averaged over four shedding cycles and the location chosen so as to cover the near as well as the downstream wake region. The spectra show more than six orders of magnitude decay at all of these locations demonstrating that 32 azimuthal points are quite sufficient for resolving the azimuthal structure of the wake at this Reynolds number.

Since we are interested here in understanding the momentum and energy transport in the wake of a sphere immersed in an oscillatory flow field, we have computed the Reynolds normal stresses and kinetic energy associated with natural vortex shedding for Re_d = 350. These statistics have been computed in a cylindrical (ϱ, φ, x) coordinate system, where the axis of this coordinate system coincides with the wake centerline and ϱ is the radial coordinate measured from this axis. In Figure 8 we show the distribution of the three normal Reynolds stress components $(\overline{u_x'^2}, \overline{u_\rho'^2}, \overline{u_\varphi'^2})$ where u' denotes the nondimensional velocity fluctuation. The fluctuating velocity is normalized by U_∞ and the fluctuations have been defined from corresponding average values, which have been computed by averaging over time as well as the azimuthal direction φ. Also shown in Figure 8 is the nondimensionalized fluctuation kinetic energy which is defined as $\overline{k} = \frac{1}{2}(\overline{u_x'^2} + \overline{u_\rho'^2} + \overline{u_\varphi'^2})$.

The streamwise and radial stresses are distributed in a manner similar to the streamwise and cross-flow stress distribution in the wake of the cylinder (Mittal and Balachandar, 1995a). Thus, even though the vortex shedding in the sphere wake is significantly different from that in the wake of a cylinder, the overall effect of vortex shedding on momentum transport is similar in both wakes. There is, however, a difference in the relative magnitudes of these two stress components. In cylinder wakes the cross-flow normal stress has the larger magnitude, whereas in the sphere wake the streamwise stress is larger. At higher Reynolds numbers, however, the wake becomes more isotropic and all normal stresses are of comparable magnitude (Leder, 1993). Furthermore, the overall stress level in the sphere wake is about an order of magnitude lower than the cylinder wake at similar Reynolds numbers (Mittal and Balachandar, 1995a), indicating that vortex shedding in the sphere wake is a significantly weaker phenomenon. This is an important observation since it suggests

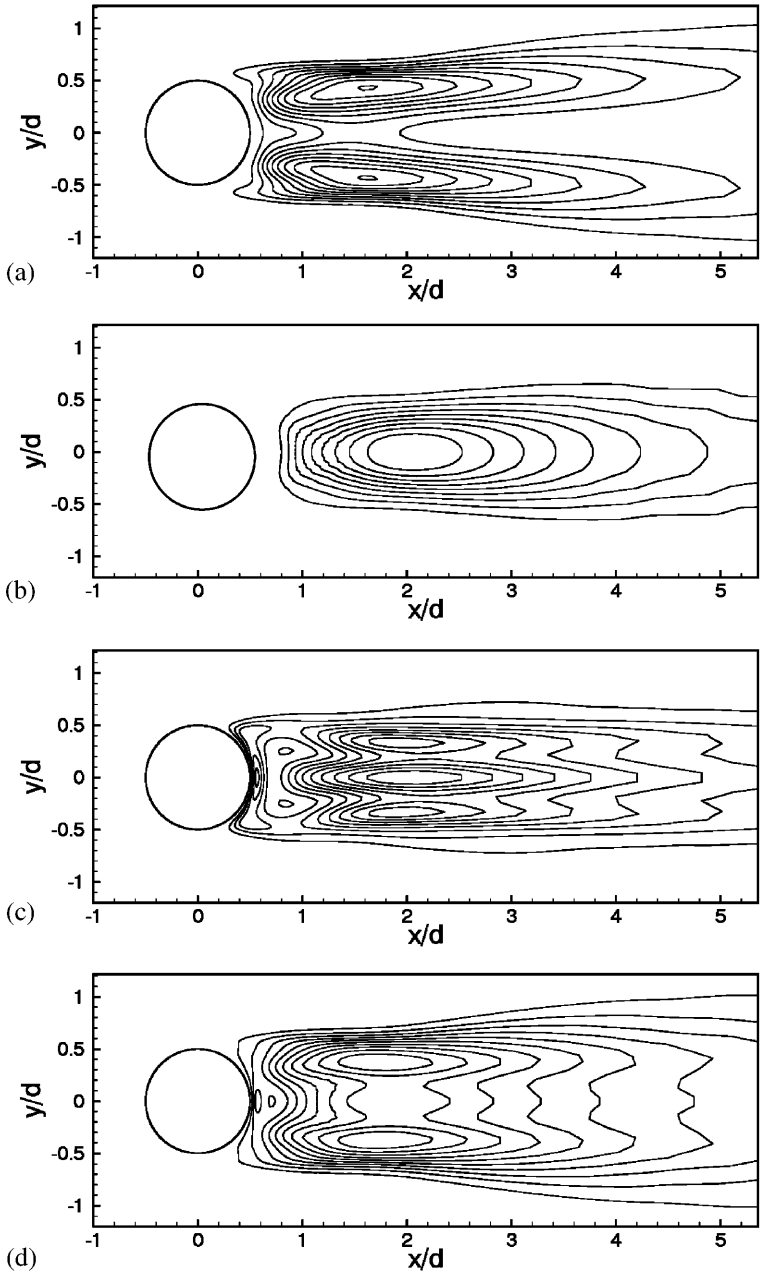

Figure 8. Contour plots of the Reynolds normal stresses that result from natural vortex shedding at Re_d = 350. The stresses have been computed in a cylindrical (ϱ, φ, x) coordinate system where the axis of this coordinate system coincides with the wake centerline and ϱ is the radial coordinate measured from this axis. (a) Streamwise normal stress $\overline{u_x'^2}$. (b) Cross-flow normal stress $\overline{u_\rho'^2}$. (c) Azimuthal normal stress $\overline{u_\varphi'^2}$. (d) Fluctuation kinetic energy $\frac{1}{2}(\overline{u_x'^2} + \overline{u_\rho'^2} + \overline{u_\varphi'^2})$.

that vortex shedding from a sphere would be quite sensitive to freestream fluctuations. Finally, we note that the maximum fluctuation kinetic energy in the wake due to natural vortex shedding is 0.026 and we denote this quantity by $k^n_{\max}$.

3.2. Sphere in Oscillatory Flow

The main objective of this study is to investigate the response of the sphere wake to freestream fluctuation and to interpret the results from the viewpoint of particle–turbulence interaction. A simple sinusoidal perturbation

is applied to one velocity component at the hemispherical inflow boundary so as to simplify the data analysis. Numerical experiments with streamwise (u_x), cross-flow (u_y), and azimuthal (u_φ) velocity perturbations indicated that, for the Reynolds number range studied here, the wake is most responsive to cross-flow velocity fluctuations and we have therefore chosen to perturb only this component. The relatively large response of the sphere wake to this perturbation is connected to the fact that the most unstable (or least stable depending on the Reynolds number) spatial mode in the sphere wake corresponds to $k_\varphi = 1$. Perturbing the u_x or u_φ sinusoidally does not produce this spatial mode but perturbing u_y does. Thus, by perturbing the u_y component of velocity, the wake is exposed to a mode that it is most unstable to and consequently a large response is produced. The velocity at the inlet is thus given by

$$\{ U_x, U_y, U_z \} = \{ 1, A_{\text{in}} \sin(2\pi\Omega t), 0 \}, \tag{3}$$

where A_{in} is the amplitude and Ω is the nondimensional frequency ($\Omega = Fd/U_\infty$ where F is the fluctuation frequency) of the perturbation. Furthermore, given the velocity fluctuation, the pressure gradient at the outer boundary can be approximated through an inviscid approximation as $\hat{\boldsymbol{n}} \cdot \nabla P^{n+1} \approx -\hat{\boldsymbol{n}} \cdot \partial \boldsymbol{U}^{n+1}/\partial t - \hat{\boldsymbol{n}} \cdot (\boldsymbol{u} \cdot \nabla \boldsymbol{u})^n$, where $\hat{\boldsymbol{n}}$ is the unit vector normal to the outer boundary. The explicit treatment of the convective term simplifies the specification of this boundary condition and all oscillatory flow simulations performed in this study employ this inhomogeneous boundary condition. However, it is worthwhile pointing out that even for the highest amplitude flow oscillation employed in the current study, simulations performed with the simple homogeneous Neumann pressure boundary condition give results which are virtually indistinguishable from those obtained using the above nonhomogeneous condition.

The procedure used in specifying the perturbation at the inlet is as follows: we choose the ambient fluctuations kinetic energy level ($\overline{k}_0$) and frequency that we would like the sphere wake to be exposed to. The corresponding amplitude of the perturbation is then given by $A_0 = 2\sqrt{\overline{k}_0}$. However, if this amplitude were to be imposed at the inlet, the perturbation level would be reduced due to viscous action and the sphere could experience a significantly attenuated fluctuation. Furthermore, the extent of this amplitude attenuation would depend on the flow Reynolds number and the fluctuation frequency. Assuming the evolution of this disturbances is governed by a linear, one-dimensional convection–diffusion equation, we can estimate that in the time it takes the perturbation to travel from the inlet to the sphere, its amplitude would reduce by a factor of $\exp(-4\pi^2\Omega^2 R_o/d\, Re_d)$, where R_0 is the radius of the outer boundary. For the various parameters considered here, the attenuation factor would have a large variation ranging from about 0.2% to 19%. In order to limit this variation and make the results more amenable to interpretation, we choose instead to amplify the inlet amplitude such that it will result in the desired ambient fluctuation level ($\overline{k}_0$) at a specified distance (l_0/d) upstream of the sphere. The amplification factor is computed from the linear analysis which gives us the following relation between the ambient fluctuation kinetic energy and the amplitude at the inlet: $A_{\text{in}} = 2\sqrt{\overline{k}_0}\exp(4\pi^2\Omega^2(R_o - l_0)/d\, Re_d)$. For all the current simulations, we have chosen $l_0/d = 5$ and our numerical simulations show that with this procedure, the desired fluctuation kinetic energy level at the specified upstream distance can be obtained to within about 3%.

Our first objective is to understand the response of the sphere wake to freestream fluctuations of different frequencies. Furthermore, we would also like to understand the effect of the Reynolds number on the response of the wake. We therefore choose two Reynolds numbers: $Re_d = 150$, which represents the situation where the wake is stable and axisymmetric, and $Re_d = 350$ where the sphere wake exhibits natural vortex shedding. For each of these Reynolds numbers we have carried out a sequence of simulations where in each simulation the sphere is exposed to a monochromatic fluctuation of a specified frequency. Each simulation is continued until a stationary state is obtained and statistics are subsequently obtained by sampling over a time interval of about six time periods of the velocity fluctuation.

3.2.1. Wake Response at $Re_d = 150$

In this first sequence of simulations we impose an ambient fluctuation with level $\overline{k}_0$ equal to 0.005 (corresponding to a 10% r.m.s. fluctuation) and Ω is varied from 0.03 to 0.2. In Figure 9 we have plotted contours of azimuthal vorticity ω_φ for $Re_d = 150$ and $\Omega = 0.03$, 0.10, and 0.02, respectively. We observe in Figure 9(a) that the lowest frequency fluctuation primarily has the effect of undulating the separated shear layers in the wake. However, the shear layers have sufficient time to respond to the low frequency perturbation and

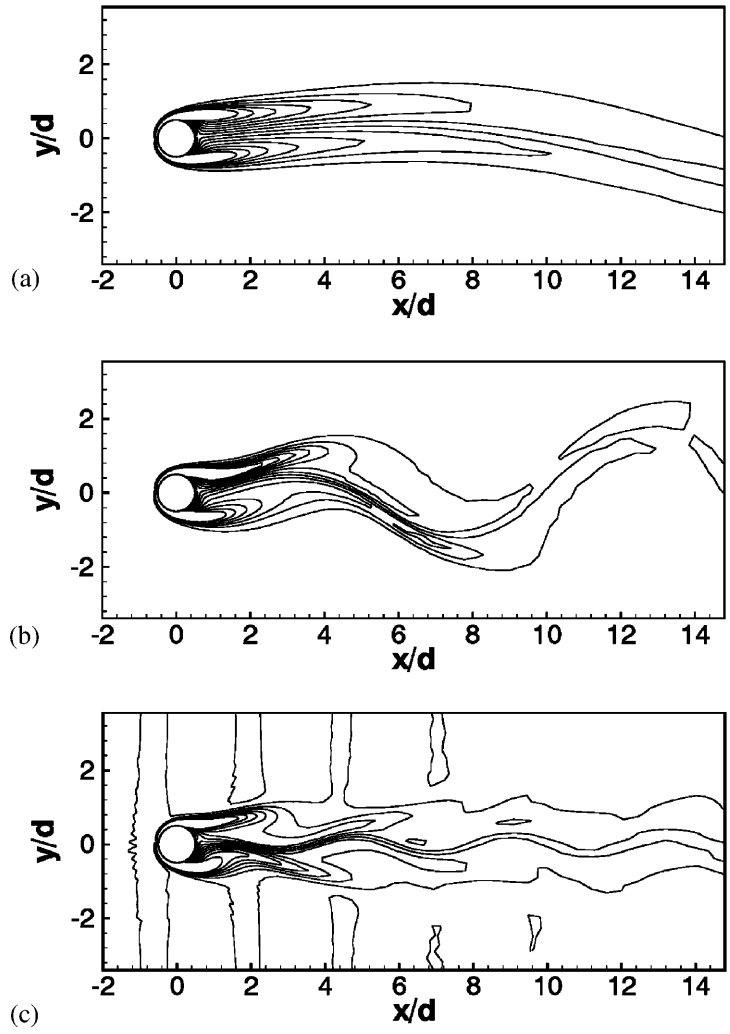

Figure 9. Contour plots of azimuthal vorticity showing the response of the shear layers to freestream fluctuations of different frequencies for Re_d = 150. The freestream fluctuation kinetic energy level is $\overline{k}_0$ = 0.005. (a) Ω = 0.03, (b) Ω = 0.10, (c) Ω = 0.20.

the perturbation does not produce any significant interaction between the two shear layers. Consequently, the shear layers maintain their integrity even in the presence of these perturbations. In contrast, the highest frequency fluctuation (Ω = 0.20) does not produce any significant large-scale motion in the separated shear layers. Instead, as evident from Figure 9(c), its primary effect is to "jitter" the shear layers and produce small-scale structures which dissipate quickly as they convect downstream.

The fluctuation with the intermediate frequency of Ω = 0.10 has by far the most dramatic effect on the separated shear layers, as is shown in Figure 9(b). Under the effect of this fluctuation, the shear layers exhibit a strong flapping motion and vorticity cancellation in regions where the shear layers from the opposite sides of the wake are brought close together results in the breaking up of the shear layer into distinct structures which subsequently convect downstream. That these convecting structures are identifiable vortices and not just regions of high vorticity can be seen from Figure 10 where we show a flow visualization of the wake for the Ω = 0.10 case. The figure shows that the patches of vorticity breaking off from the shear layers are in fact Λ-shaped vortices which are formed in the near wake and which decay slowly as they convect downstream. The topology of these vortices is quite different from that observed in natural vortex shedding (Figure 6). In particular, the connected vortex loops which characterized natural vortex shedding at higher Reynolds numbers are not present in the forced wake. Thus, even though a perturbation of a suitable frequency induces the formation of distinct vortex structures in the near wake, this phenomenon has no connection with natural vortex shedding.

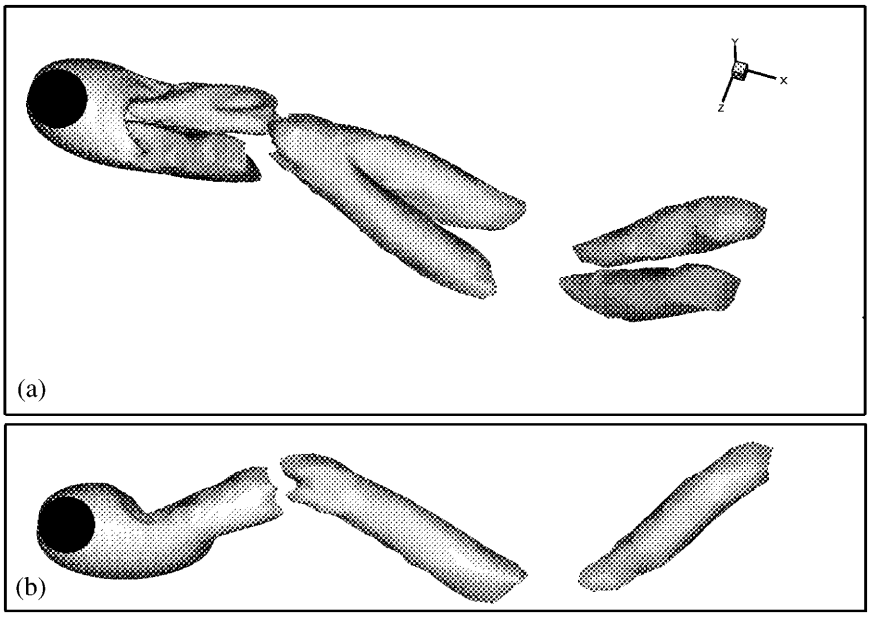

Figure 10. Visualization of the three-dimensional vortex topology in the forced wake at Re_d = 150. The fluctuation frequency corresponds to Ω = 0.10 where the wake shows a significant response. A perspective as well as a side view of the wake is shown and distinct Λ-shaped vortices can be observed in the near wake.

The perturbation of the shear layer by the freestream fluctuation induces fluctuations in the velocity and this results in the production of fluctuation kinetic energy in the near wake. In a particulate flow, this energy is transported from the near wake into the surrounding fluid and can lead to enhancement of turbulence. Thus, a particle's ability to enhance turbulence is directly related to the fluctuation kinetic energy produced in its wake. In Figure 11 we have plotted contours of fluctuation kinetic energy normalized by $\overline{k}_0$ for the Re_d = 150 case. The three plots correspond to Ω = 0.03, 0.1, and 0.2, respectively, and have been obtained by averaging the flow over about six periods of the fluctuation. This plot shows that, for all perturbation frequencies, the sphere acts to amplify the freestream fluctuations, and kinetic energy levels significantly higher than the ambient level of 0.005 are found in the near wake. Furthermore, we find that the maximum kinetic energy in the wake ($k_{\max}$) varies significantly with the perturbation frequency and the maximum kinetic energy in the wake is obtained for the Ω = 0.1 case. For this case we find a maximum energy level of 0.0275 which is higher than the ambient level by a factor of 5.5. In Figure 12 we have plotted ($k_{\max}/\overline{k}_0$) versus the perturbation frequency and this plot indicates a maximum at about Ω = 0.1. The high value of fluctuation kinetic energy in the wake can be directly attributed to the strong response of the wake at this frequency. At higher and lower frequencies, the response of the wake is quite limited and this results in a lower amplification of the freestream perturbations.

To understand the response of the wake to the fluctuation amplitude, a separate series of simulations have been carried with an ambient fluctuation level of 0.00125 (corresponding to a 5% r.m.s. fluctuation) and in Figure 12 we have also plotted ($k_{\max}/\overline{k}_0$) versus the perturbation frequency for this case. It is clear from this plot that the response of the wake at both fluctuation levels is quite similar with the maximum amplification of freestream fluctuation energy occurring at Ω = 0.1. However, the amplification factor at this frequency is about 6.8, which is somewhat higher than obtained previously for the $\overline{k}_0$ = 0.005 case. At higher and lower frequencies, the amplification factor is quite similar to that obtained for the previous case. Thus, near the frequency of maximum amplification, the wake does not respond linearly to the fluctuation level but otherwise we find that the response does not depend significantly on the fluctuation level.

3.2.2. Wake Response at Re_d = 350

In order to understand the wake response in the flow regime where natural vortex shedding occurs, we have carried out a separate sequence of simulations at Re_d = 350. The Strouhal number of natural vortex

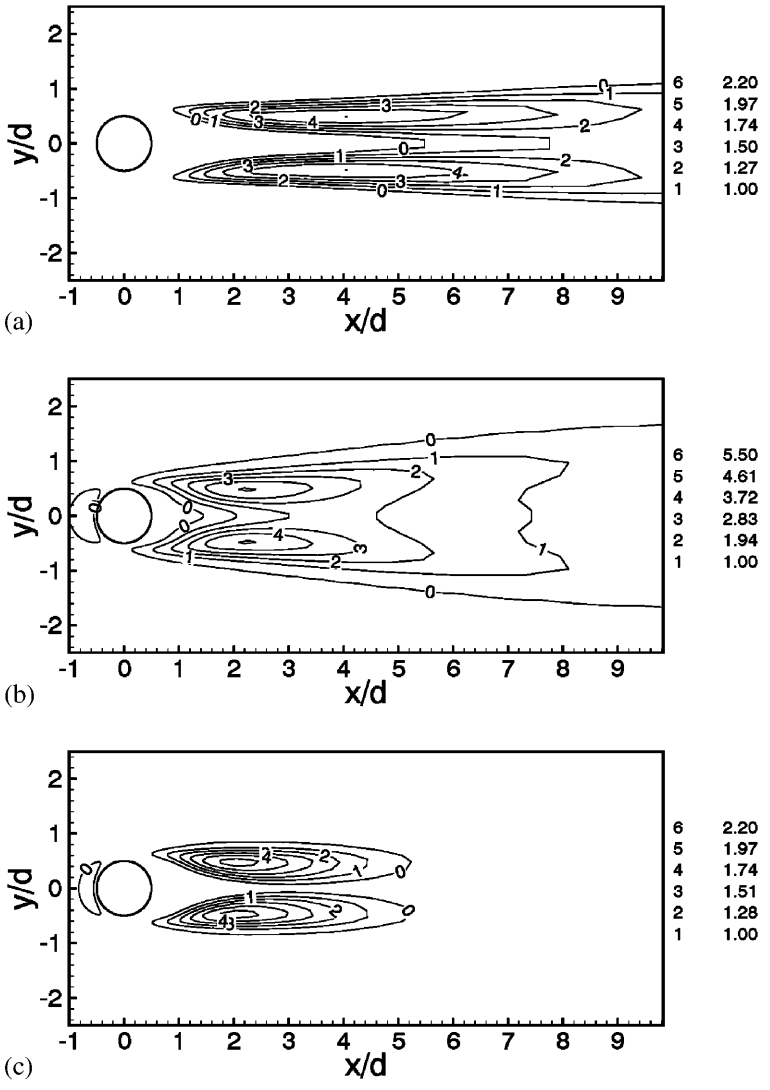

Figure 11. Contour plots showing the variation of mean fluctuation kinetic energy normalized by $\overline{k}_0$ in the forced wake at Re_d = 150. The freestream fluctuation kinetic energy level is $\overline{k}_0$ = 0.005. (a) Ω = 0.03, (b) Ω = 0.10, (c) Ω = 0.20.

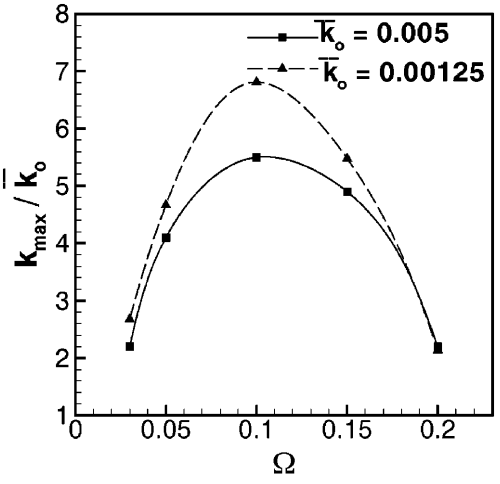

Figure 12. Variation of the maximum fluctuation kinetic energy normalized by $\overline{k}_0$ with the fluctuation Strouhal number Ω for the forced wake at Re_d = 150.

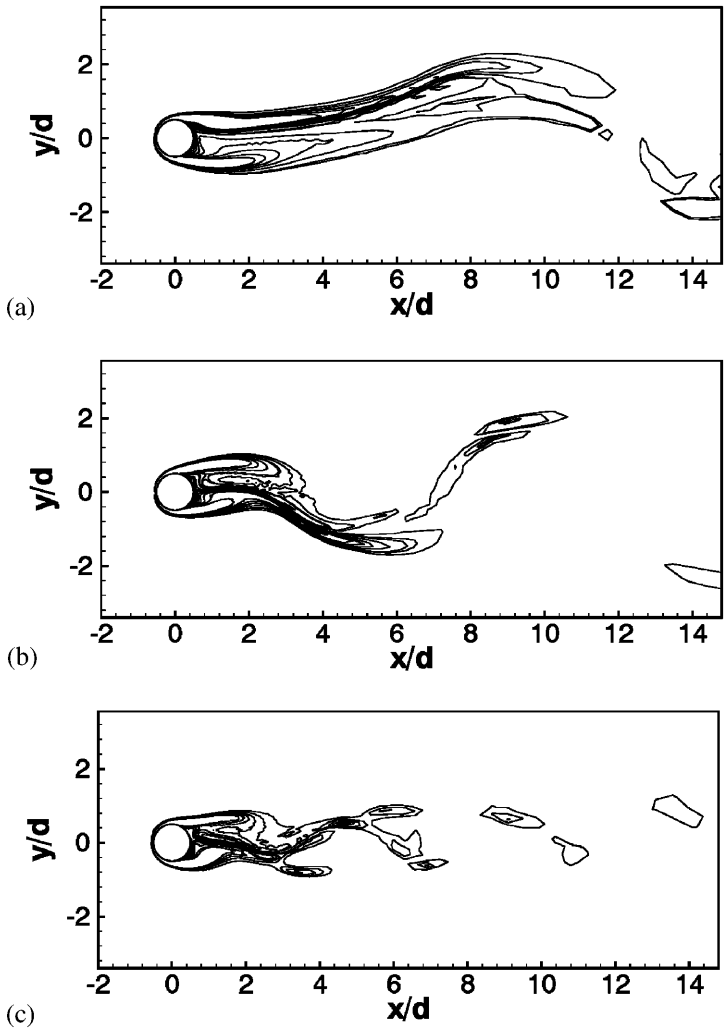

Figure 13. Contour plots of azimuthal vorticity showing the response of the shear layers to freestream fluctuations of different frequencies for Re_d = 350. The freestream fluctuation kinetic energy level is $\overline{k}_0$ = 0.005. (a) Ω = 0.05, (b) Ω = 0.10, (c) Ω = 0.20.

shedding at this Reynolds number is about 0.14 and here we have carried out simulations within the range $0.05 \leq \Omega \leq 0.2$. Two different freestream fluctuation levels with $\overline{k}_0$ = 0.005 and 0.00125 have been used and these correspond to r.m.s fluctuations of 10% and 5%, respectively.

In Figure 13 we have plotted contours of azimuthal vorticity ω_φ for Ω = 0.05, 0.10, and 0.02 for $\overline{k}_0$ = 0.005. Comparison of these plots with Figure 9 indicates that the response of the wake is in general similar to that found at the lower Reynolds numbers. Low frequency perturbations tend to produce waviness in the shear layers, whereas high frequency perturbations produce relatively smaller-scale distortions. The intermediate frequency of 0.10 produces the most significant response and Figure 13b shows the streamwise oriented vortices formed in the near wake at this frequency. This observation is also supported by a three-dimensional flow visualization of the vortex topology for this case which is shown in Figure 14. This figure shows the formation of compact streamwise-oriented Λ-shaped vortices which separate from the shear layers and convect downstream. For the most part, the topology of the structures observed here is qualitatively similar to that observed for the lower Reynolds number case. However, we find that in addition to the large Λ-shaped vortices, another pair of weak streamwise vortices are also formed periodically in the wake. A comparison of this figure with Figure 6 shows that the forced wake does not exhibit the connected vortex-loop-type topology indicating that natural vortex shedding is for the most part suppressed in this unsteady environment.

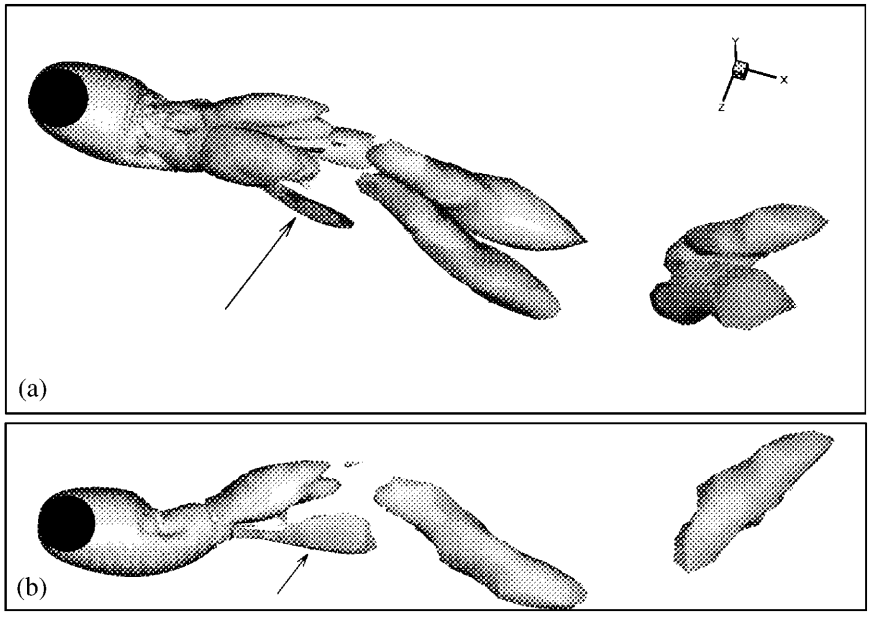

Figure 14. Visualization of the three-dimensional vortex topology in the forced wake at Re_d = 350 for $\overline{k}_0$ = 0.005. The fluctuation frequency corresponds to Ω = 0.10 where the wake shows the largest response. A perspective as well as a side view of the wake is shown and Λ-shaped vortices similar to those present in Figure 10 can be observed. The arrows indicate the additional pair of streamwise vortices that are observed in this forced wake.

Statistics have also been accumulated for these simulations and Figure 15 shows the distribution of the normalized fluctuation kinetic energy in the wake for three different forcing frequencies. As for the low Reynolds number case we find that the large response of the wake at Ω = 0.10 results in a high level of fluctuation kinetic energy. In Figure 16 we have plotted ($k_{\max}/\overline{k}_0$) versus the perturbation frequency for this Reynolds number. In order to locate the maximum of this curve more precisely, an additional simulation has been carried out at Ω = 0.125. The spline fit through these points indicates that the maximum kinetic energy is produced at Ω = 0.106, where the ambient fluctuation kinetic energy is amplified by a factor of about 14.7. At higher and lower frequencies too there is significant amplification with the lowest amplification factor of about 10 for Ω = 0.20. The amplification at all frequencies is significantly higher than that obtained at the lower Reynolds number and this is mainly due to the fact that, at higher Reynolds numbers, the vorticity in the shear layers is of a higher magnitude and when these shear layers move under the influence of the imposed perturbations, they induce larger velocity perturbations. In Figure 16 the solid horizontal line indicates the magnitude of the maximum kinetic energy associated with natural vortex shedding normalized by $\overline{k}_0$ = 0.005, and this clearly shows that all of the frequencies imposed here produce a fluctuation level which is higher than that produced by natural vortex shedding. It should be reemphasized that the highest amplification is found not at the natural vortex shedding frequency of about 0.14 but at a lower frequency of 0.106. This further supports the assertion that with this amplitude of perturbation, natural vortex shedding does not play a significant role in the amplification process.

In contrast to the forced wake at the lower Reynolds number, we expect the wake at this higher Reynolds number to behave in a more complicated manner as the amplitude of the perturbation is reduced. This is because in the limit of a very small perturbation we expect natural vortex shedding to reappear and affect the momentum and energy transport in the wake. In order to understand the wake response in this regime, another sequence of simulations has therefore been carried out with $\overline{k}_0$ = 0.00125, which corresponds to a 5% r.m.s. fluctuation. In Figure 16 we have also plotted the amplification factor for this sequence and a number of interesting observations can be made regarding this curve. The kinetic energy of the ambient fluctuations is amplified quite dramatically; up to a factor of about 38.6 for Ω = 0.15. The normalized maximum kinetic energy obtained for natural vortex shedding is also indicated by the dashed horizontal line and we observe that all of the imposed perturbations produce a maximum kinetic energy which is higher

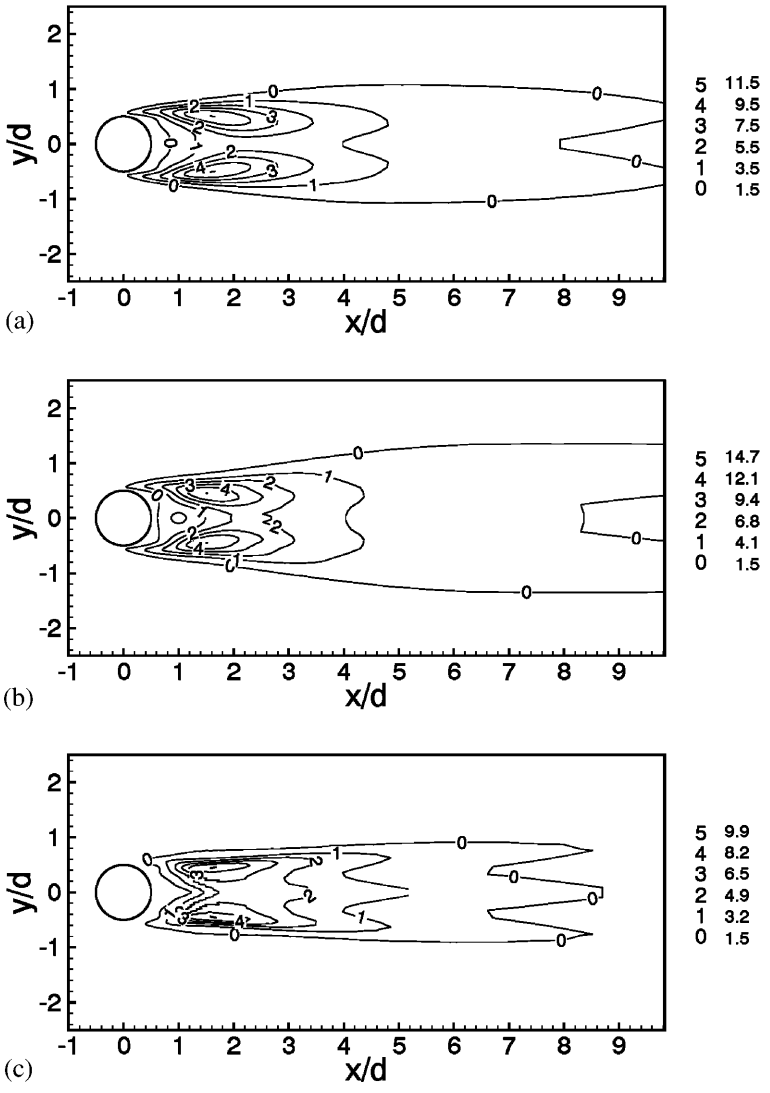

Figure 15. Contour plots showing the variation of mean fluctuation kinetic energy normalized by $\overline{k}_0$ in the forced wake at Re_d = 150. The freestream fluctuation kinetic energy level is $\overline{k}_0$ = 0.005. (a) Ω = 0.05, (b) Ω = 0.10, (c) Ω = 0.20.

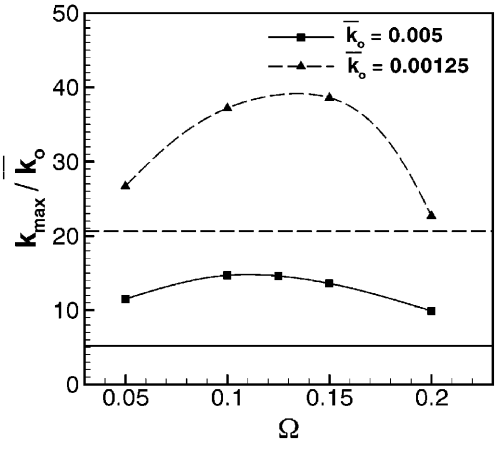

Figure 16. Variation of the maximum fluctuation kinetic energy normalized by $\overline{k}_0$ with the fluctuation Strouhal number Ω for the forced wake at Re_d = 350. The solid and dashed horizontal lines indicate $(k^n_{\max}/\overline{k}_0)$ for $\overline{k}_0$ = 0.005 and 0.00125, respectively.

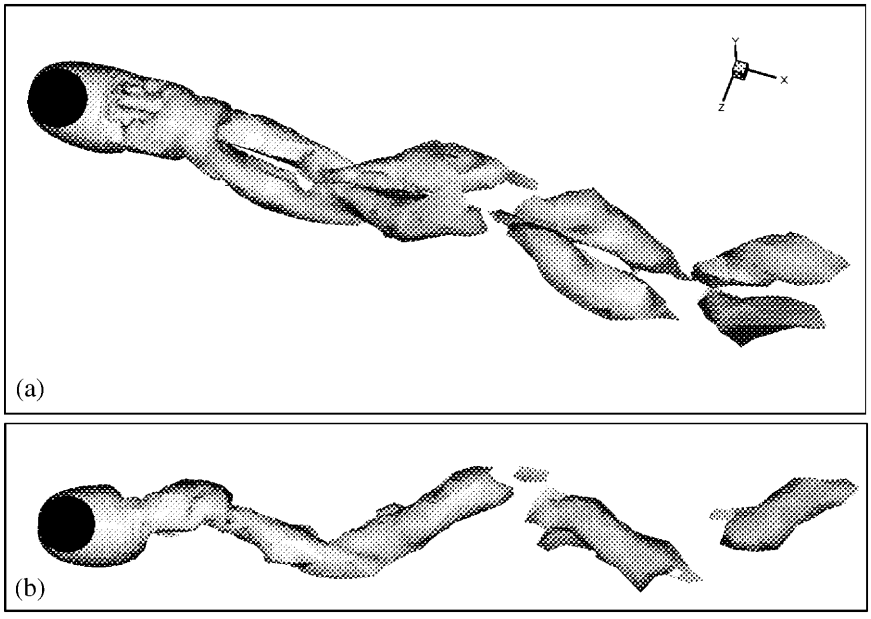

Figure 17. Visualization of the three-dimensional vortex topology in the forced wake at Re_d = 350 for $\overline{k}_0$ = 0.00125. The fluctuation frequency corresponds to Ω = 0.15 where the wake shows the strongest response. A perspective as well as a side view of the wake is shown. The wake topology is similar to that of a naturally shedding wake indicating that natural vortex shedding is not disrupted at this lower fluctuation level.

than that produced due to natural vortex shedding. In fact, for Ω = 0.15, the maximum kinetic energy in the wake is greater than that produced by natural vortex shedding by a factor of about 2.

The spline put through the data points in Figure 16 also indicates that the largest amplification occurs at a frequency of about 0.141, which is higher than the frequency at which maximum amplification is obtained for $\overline{k}_0$ = 0.005. This is in contrast to the behavior observed for Re_d = 150, where the frequency for maximum amplification does not change with the fluctuation level. The fact that this frequency of maximum amplification matches with the natural vortex shedding frequency suggests that, at this lower fluctuation level, natural vortex shedding has a dominant presence in this forced wake. In order to confirm this we have plotted flow visualizations for this case in Figure 17 and we find that the vortex topology in this case is significantly different from that observed for $\overline{k}_0$ = 0.005. The wake clearly exhibits the connected loop structure similar to that observed in the naturally shedding wake (Figure 6) indicating that the fluctuation level of $\overline{k}_0$ = 0.00125 is not high enough to suppress natural vortex shedding completely. However, the maximum kinetic energy in the forced wake is significantly higher than that found in the naturally shedding wake and this suggests that the dynamics in the forced wake is not completely determined by natural vortex shedding. It seems that the forcing and natural vortex shedding act together to produce a large-scale fluctuation in the near wake resulting in a high magnitude of fluctuation kinetic energy.

Wu and Faeth (1995) found that low-level freestream turbulence (4% turbulence intensity) does not have a significant effect on the natural vortex shedding process in the wake of a sphere. Our simulations also indicate that natural vortex shedding is not suppressed even in the presence of a 5% fluctuation in the transverse velocity. In order to investigate further the effect of the perturbation amplitude on natural vortex shedding, we have performed a sequence of simulations at Re_d = 350 with Ω = 0.20 where the perturbation amplitude has been systematically varied from a small to a relatively large magnitude. A forcing frequency different from the natural shedding frequency has been chosen for these simulations in the hope that it will allow us to differentiate between phenomena associated with natural vortex shedding and the imposed fluctuation. Simulations have been carried out with $\overline{k}_0$ = 0.0002, 0.00125, 0.0028, and 0.005 which correspond to 2%, 5%, 7.5%, and 10% r.m.s. perturbations in the transverse velocity.

In Figure 18 we have plotted the $(k_{\max}/k^n_{\max})$ versus $\overline{k}_0$ and a spline has been fit through the data points. The plot shows that up to about $\overline{k}_0$ = 0.001 (4.5% fluctuation level), the maximum kinetic energy in the wake is within about 5% of $k^n_{\max}$. As the flucutation level is increased further, there is a steep increase in

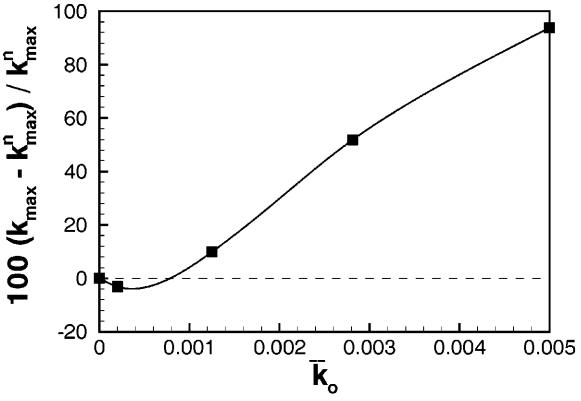

Figure 18. Relative increase in maximum kinetic energy in the forced wake ($k_{\max}$) over the maximum kinetic energy observed in the naturally shedding wake ($k^n_{\max}$) versus the freestream fluctuation kinetic energy level.

the maximum kinetic energy and we find that at $\overline{k}_0$ = 0.00125, the maximum kinetic energy is roughly 10% higher than $k^n_{\max}$. The steep increase in the maximum kinetic energy indicates that freestream fluctuation is beginning to affect the natural vortex shedding process. However, since the maximum kinetic energy is not substantially different from that obtained from natural vortex shedding, it is also apparent that the natural vortex shedding is affected only slightly by the freestream fluctuations. Thus for fluctuations with the level of about $\overline{k}_0$ = 0.00125, the wake dynamics is still determined for the most part by natural vortex shedding. Beyond $\overline{k}_0$ = 0.00125, the maximum kinetic energy continues its steady rise with the fluctuation level and at $\overline{k}_0$ = 0.0028, $k_{\max}$ is about 50% higher than $k^n_{\max}$. This indicates that at this fluctuation level the natural vortex shedding is substantially affected by the freestream fluctuation and the momentum and energy exchange in the wake is a combined effect of natural vortex shedding and the wake response to the freestream fluctuations. Finally, at $\overline{k}_0$ = 0.005, the maximum kinetic energy is about 94% higher than the maximum kinetic energy associated with natural vortex shedding. The significantly higher maximum kinetic energy along with previous flow visualizations shows that at at this level of freestream fluctuations natural vortex shedding is disrupted completely by the freestream fluctuations and the wake dynamics is determined almost exclusively by the forced response of the wake.

3.2.3. Reynolds Number Dependence of Wake Response

Figures 12 and 16 clearly show that the maximum fluctuation kinetic energy in the wake can increase significantly with the particle Reynolds number. This is in line with the observations of Hetsroni (1989) that higher particle Reynolds numbers are correlated with turbulence enhancement. In this context, it is of interest to investigate systematically the effect that the particle Reynolds number has on turbulence enhancement. In order to isolate the effect of the Reynolds number on the wake response, it is desirable to fix the perturbation frequency. However, given that the frequency of maximum kinetic energy amplification is itself Reynolds number dependent, it is not clear what particular value of frequency should be chosen. Our approach here is to use a perturbation with a narrow frequency band which covers the maximum amplification frequency for the Reynolds number range of interest in the current study. In particular, the inlet perturbation we employ is of the form

$$U_y(t) = \sum_{m=1}^{3} A^m_{\text{in}} \sin\{2\pi\Omega_m(t - T_m)\} \tag{4}$$

and we choose Ω_1 = 0.007, Ω_2 = 0.11, and Ω_3 = 0.15. Furthermore, in order to minimize the skewness in the perturbation signal we choose a time lag $T_m = (m-1)/3\Omega_1$ and A^m_{in} is chosen such that each frequency contributes equally to the net kinetic energy ($\overline{k}_0$) at the reference location (l_0). Figure 19 shows the temporal variation of the cross-flow velocity perturbation that results from this procedure. We have fixed the total freestream fluctuation kinetic energy level and carried out a sequence of six simulations over a range of Reynolds numbers from 100 to 350. Two such sequences have been simulated; the first with $\overline{k}_0$ = 0.00125 and the second with $\overline{k}_0$ = 0.005.

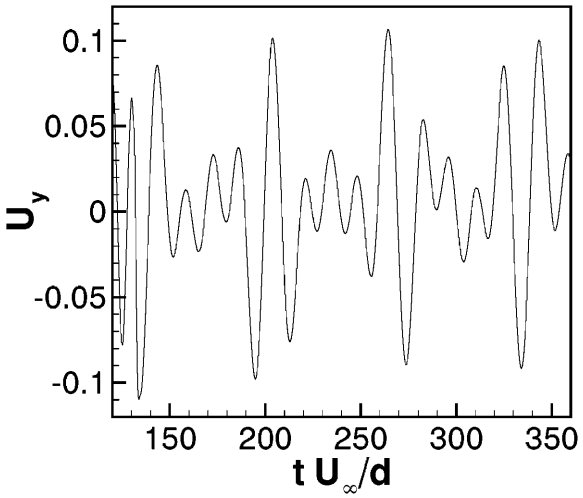

Figure 19. Temporal variation of the cross-flow velocity perturbation used in studying the effect of Reynolds number on the amplification of kinetic energy in the sphere wake. This fluctuation is generated by linearly combining fluctuations with Ω = 0.07, 0.11, and 0.15.

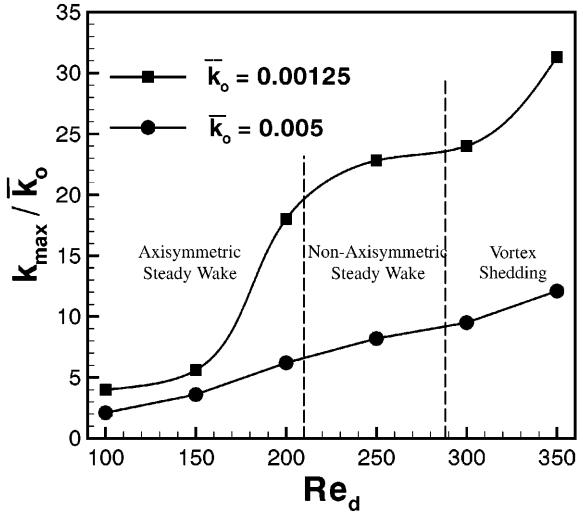

Figure 20. Variation of the normalized maximum kinetic energy ($k_{\max}/\overline{k}_0$) with the flow Reynolds number.

For each of these simulations, the accumulation of statistics follows a procedure similar to that used in the previous section. Figure 20 shows a plot of ($k_{\max}/\overline{k}_0$) versus the Reynolds number. For the $\overline{k}_0$ = 0.00125 case we find that the plot has a relatively complex variation with Reynolds number. In particular there are two Reynolds number ranges where there is a rapid increase of $k_{\max}$ with Reynolds number. The first is in the vicinity of Re_d = 200 and the second occurs at around Re_d = 300. Our understanding of a sphere immersed in a uniform steady flow suggests that the first increase is connected with the bifurcation from axisymmetric to the nonaxisymmetric double-thread wake regime which occurs at around Re_d = 210. Similarly, the second increase in $k_{\max}$ is connected with the wake becoming susceptible to natural vortex shedding at around Re_d = 300. As pointed out earlier, the k_φ = 1 mode is destabilized at each of these bifurcations and the growth of this mode is further encouraged by the freestream perturbations. Thus, as the Reynolds number is increased and the wake bifurcates to increasingly complex and unstable regimes, low-level freestream fluctuations tend to produce larger perturbations in the attached shear layers and consequently lead to a substantial increase in the fluctuation kinetic energy.

The behavior at the higher freestream fluctuation level of k_0 = 0.005 is however markedly different. We find that the maximum kinetic energy in the wake increases almost linearly with the Reynolds number

for this case, and the rate of increase of $k_{\max}$ is clearly insensitive to the state of the natural wake at the given Reynolds number. This is in line with our previous results which indicate that high-level freestream fluctuations completely overwhelm the natural behavior of the wake. This is also further corroborated by our previous finding that maximum amplification of incident energy at this fluctuation level occurs close to $\Omega = 0.1$ and this value does not vary significantly with the Reynolds number. Therefore the wake response to this high-level freestream fluctuation is primarily determined by the resonance of the shear layers and this response remains qualitatively the same over the whole range of Reynolds numbers studied here.

4. Discussion

The various findings of the current study can now be summarized and interpreted in the context of particle–turbulence interaction. Even at low Reynolds numbers where the wake is not susceptible to natural vortex shedding, freestream fluctuations can induce flapping and breakup of the separated shear layers and this can lead to the formation of compact vortices in the near wake. The perturbation in the shear layers and the formation of the compact vortices induces large velocity perturbations in the near wake, and fluctuation kinetic energy levels significantly higher than the incident fluctuation can be produced. At higher Reynolds numbers a similar scenario is observed and there is an even higher amplification of the incident kinetic energy.

Forcing the wake at different frequencies and amplitudes shows that the sphere wake acts primarily like an oscillator and returns large amounts of energy to the flow at resonance. At low Reynolds numbers, where the wake is not susceptible to natural vortex shedding, this oscillator-type behavior is observed for small as well as large fluctuation levels. In contrast, at high Reynolds numbers, where the wake is susceptible to natural vortex shedding, the simple oscillator-type behavior is only observed for large freestream fluctuation levels ($\gtrsim$ 7% r.m.s.). At these high fluctuation levels, natural vortex shedding is completely disrupted and the wake response to freestream fluctuations is qualitatively similar to that obtained at low Reynolds numbers. However, at low fluctuation levels, natural vortex shedding is not completely suppressed and the wake response is more complicated. In the regime where the wake acts like a simple oscillator, it is found that the wake resonates at a nondimensional frequency of about 0.1 and, in the Reynolds number range studied here, this value does not vary significantly with the Reynolds number. At higher Reynolds numbers and low fluctuation levels where natural vortex shedding is present, the frequency of maximum kinetic energy amplification is closer to the natural shedding frequency. This behavior of the forced wake is shown schematically in Figure 21.

The current simulations show that the amplification of kinetic energy attains a maximum at the resonant frequency and then decreases as the perturbation frequency is increased. The Strouhal number corresponding to the resonance frequency is in the range between 0.1 and 0.14 which matches well with the frequency of natural vortex shedding at low Reynolds numbers (Figure 2). The fact that the resonance frequency is comparable with the natural vortex shedding frequency at low Reynolds numbers is not a coincidence. As shown by Roshko (1955) for cylinder wakes, the vortex shedding frequency scales with a velocity and length scale associated with the wake and we expect the same time scale to be relevant in the case of the forced wake. Thus the resonance frequency is expected to be comparable with the frequency observed in the naturally shedding wake. Therefore the lowest frequency that the sphere wake is expected to be responsive to is about 0.1. Furthermore, this also suggests that at higher Reynolds numbers, where the high mode of shedding is active, the wake will also resonate at high frequencies associated with this shedding mode. Thus, depending on the particle Reynolds number, the nondimensional resonance frequency is expected to vary from 0.1 to about 1.0 and significant kinetic energy could be produced in the wake over this range of freestream frequencies. Our forced wake simulations are currently limited to lower Reynolds numbers due to resolution requirements and we have therefore not been able to analyze the response of the forced wake in the range of Reynolds numbers where the high mode is present.

Our observations now allow us to hypothesize an explanation for the findings of Gore and Crowe (1989). As shown in Figure 1, Gore and Crowe have suggested that particles enhance turbulence when the particle-to-eddy size ratio is greater than about 0.1. Using Taylor's frozen-field hypothesis, the eddy size l_e can be written in terms of an eddy frequency f_e as $l_e = U_\infty / f_e$ and the condition for amplification of ambient turbulence

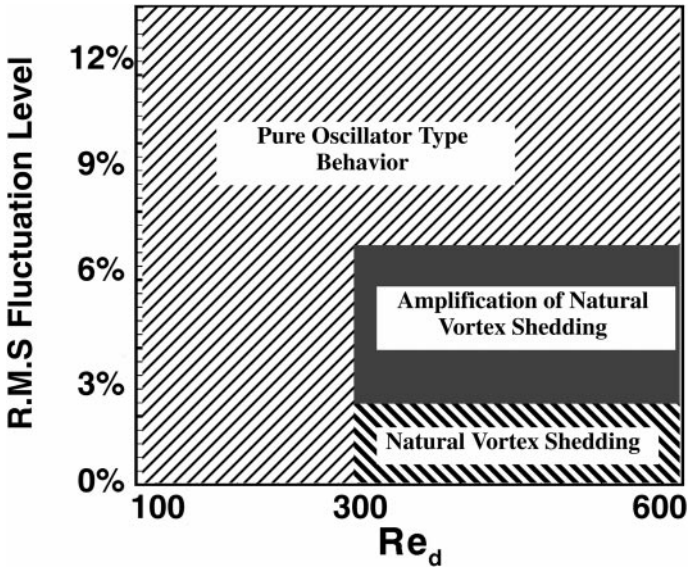

Figure 21. Schematic showing the various regimes observed in the wake of a sphere immersed in a sinusoidally oscillating freestream.

is then equivalent to $\Omega_e \gtrsim 0.1$ where Ω_e is the nondimensional eddy frequency given by $\Omega_e = f_e d/U_\infty$. As argued in the previous paragraph, this is precisely the frequency range where we expect a resonant response from the wake. A possible explanation for the findings of Gore and Crowe therefore is that turbulence is enhanced when the eddy frequency lies in a range of resonance of the sphere wake, i.e., when $\Omega_e \gtrsim 0.1$. In this range the freestream turbulence is very effective in destabilizing the wake, and this results in the development of compact vortices and significant amplification of the turbulence kinetic energy of the carrier fluid.

The current simulations also suggest that the phenomenon of enhancement of turbulence by particles is not governed by a single parameter. We have found that the degree to which turbulence can be enhanced by a single particle depends on the particle Reynolds number, the particle-to-eddy size ratio and the intensity of the freestream fluctuation. Obviously in a particulate flow with many particles, the degree to which turbulence is enhanced will also depend on the particle volume-fraction. This dependance of turbulence enhancement on multiple parameters is clearly inline with Figure 1 which shows a wide variation in the degree to which turbulence is enhanced for a given particle-to-eddy size ratio.

5. Conclusions

Based on our simulations the following conclusions can be made:

- Natural vortex shedding from particles seems capable of significantly enhancing the turbulence in the surrounding fluid but this mechanism is only active when the particle Reynolds number is greater than about 300 and the freestream turbulence level is low. High-level freestream fluctuations tend to suppress natural vortex shedding and therefore it is unlikely that natural vortex shedding plays a significant role in turbulence enhancement in highly turbulent flows.
- In the presence of freestream fluctuations, the sphere wake behaves like an oscillator and returns large amounts of energy to the surrounding fluid at resonance. This mechanism is not connected with natural vortex shedding and can therefore be activated even when the particle Reynolds number is significantly lower than 300. If natural vortex shedding is present and the freestream fluctuation level is low, this mechanism can also amplify the effect of vortex shedding. Furthermore, this mechanism might be solely responsible for turbulence enhancement in the high particle Reynolds number, high turbulence level regime where the natural vortex is completely disrupted.

- In the Reynolds number range from 100 to 350 which has been studied here, the Strouhal number at which the wake resonates varies between 0.1 and 0.14 and this is comparable with the natural vortex shedding Strouhal number. At higher particle Reynolds numbers it is expected that the individual shear layers will also become susceptible to resonance at higher frequencies and therefore amplification of turbulent kinetic energy should be observed at Strouhal numbers significantly greater than 0.1.
- The behavior of the forced wake observed here also provides a possible explanation for the observations of Gore and Crowe that turbulence is enhanced when the ratio of particle-to-eddy size is roughly greater than 0.1. This size ratio when reinterpreted as the Strouhal number of the energy containing eddies of turbulence implies that turbulence is enhanced when the Strouhal number corresponding to the passage of energy containing turbulent eddies is greater than 0.1. Since our simulations indicate that this is precisely the resonant range of the wake, the behavior observed by Gore and Crowe may therefore be attributed to the resonance between the turbulent fluctuations and the particle wake.

Our final objective is to obtain a better understanding of the mechanisms that are responsible for turbulence enhancement in particulate flows and to use this for developing models for predicting the effect of particles on turbulent flows. Considerable simplifications have been made in our numerical study in modeling the interaction of particles with turbulence and these have been necessitated by the need to cover a large, multidimensional parameter space. Despite these simplifications we believe that some key mechanisms have been identified and future work will be directed toward studying these mechanisms further in a more realistic setting.

Acknowledgment

These simulations have been performed on the CRAY T-90 at the San Diego Supercomputer Center and on the Origin 2000 at NCSA. I would like to acknowledge Professors R.W. Mei and W.G. Tiederman who read the manuscript and provided useful comments. The code was ported to the Origin platform by Dr. F.M. Najjar and his help is gratefully acknowledged.

References

Achenbach, E. (1974). Vortex shedding from spheres, *J. Fluid Mech.*, **62**(2), 209–221.
Bloor, M.S. (1964). The transition to turbulence in the wake of a circular cylinder, *J. Fluid Mech.* **19**, 290.
Canuto, C., Hussaini, M.Y., Quarteroni, A., and Zang, T.A. (1988). Spectral methods in fluid dynamics, Springer-Verlag, Berlin.
Chorin, A.J. (1968), Numerical Solution of the Navier-Stokes Equations, *Math. Comput.*, **22**, 745–757.
Gore, R.A., and Crowe, C.T. (1989). Effect of particle size on modulating turbulent intensity, *Int. J. Multiphase Flow*, **15**(2), 279–285.
Hetsroni, G. (1989). Particles-turbulence interaction, *Int. J. Multiphase Flow*, **15**(5), 735–749.
Kim, L. Elghobashi, S., and Sirignano, W.A. (1997). Unsteady flow interactions between an advected vortex tube and a spherical particle, *J. Fluid Mech.*, **288**, 123–155.
Kim, L. Elghobashi, S., and Sirignano, W.A. (1997). Unsteady flow interactions between a pair of advected vortex tubes and a rigid sphere, *Int. J. Multiphase Flow*, **23**(1), 1–23.
Leder, A., and Geropp, D. (1993). Coherent structures in axisymmetric shear layer flows In *Near-Wall Turbulent Flows*, (R.M.C. So, C.G. Speciale and B.E. Launder, eds.) pp. 517–526. Elsevier Science Publishers.
Margavey, R.H., and Bishop, R.L. (1961). Transition ranges for three-dimensional wakes, *Can. J. Phys.*, **39**, 1418–1422.
Margavey, R.H., and MacLatchy, C.S. (1965). Vortices in sphere wakes, *Can. J. Phys*., **43**, 1649–1656.
R. Mittal (1999a). A Fourier–Chebyshev spectral collocation method for simulating flow past spheres and spheroids, *Int. J. Numer. Meth. Fluids*, **30**, 921–937.
R. Mittal (1999b). Planar symmetry in the unsteady wake of a sphere, *AIAA J.*, **37**(3), 388–391.
Mittal, R., and Balachandar, S. (1995a). Effect of three-dimensionality on the lift and drag of nominally two-dimensional cylinders, *Phys. Fluids*, **7**(8), 1841–1865.
Mittal, R., and Balachandar, S. (1995b). Generation of streamwise vortical structures in bluff-body wakes, *Phys. Rev. Lett.*, **75**(7), 1300–1303.
Mittal, R., and Balachandar, S. (1996a). Direct numerical simulation of flow past elliptic cylinders, *J. Comp. Phys.*, **124**, 351–367.
Mittal, R., and Balachandar, S. (1996b). Generation and evolution of vortical structures in bluff-body wakes, AIAA 96-0210.
Nakamura, I. (1976). Steady wake behind a sphere, *Phys. Fluids*, **19**(1), 5–8.
Natarajan, R., and Acrivos, A. (1993). The instability of the steady flow past spheres and disks, *J. Fluid Mech.*, **254**, 323–344.
Ormieres, D., and Provensal, M. (1998). Transition to turbulence in the wake of a sphere, *Phys. Rev. Lett.*, **83**(1), 80–83.

Owen, P.R. (1969). Pneumatic transport, *J. Fluid Mech.*, **39**(2), 407–432.
Pan, Y., and Bannerjee, S. (1997). Numerical investigation of the effects of large particles on wall turbulence, *Phys. Fluids*, **9**(12), 3786–3807.
Roshko, A. (1955). On the drag and shedding frequency of bluff bodies, *J. Aero. Sci.*, **22**, 124–130.
Sakamoto, H., and Haniu, H. (1990). A study of vortex shedding from spheres in a uniform flow, *J. Fluids. Engr.*, **112**, 386–392.
Sakamoto, H., and Haniu, H. (1995). The formation mechanism and shedding frequency of vortices from a sphere in uniform shear flow, *J. Fluid Mech.*, **287**, 151–171.
Tsuji, Y., and Morikawa, Y. (1982). LDV measurements of an air-solid two-phase flow in a horizonatal pipe, *J. Fluid Mech.*, **120**, 385–409.
Tsuji Y., Morikawa, Y., and Shiomi, H. (1984). LDV measurements of an air-solid two-phase flow in a vertical pipe, *J. Fluid Mech.*, **139**, 417–434.
Tsuji, Y., Morikawa, Y., Tanaka, T., Karimine K., and Nishida, S. (1988). Measurements of an axisymmetric jet laden with coarse particles, *Int. J. Multiphase Flow*, **14**, 565–574.
Yusof, J.M. (1996). Interaction of Massive Particles with Turbulence, PhD Thesis, Dept. of Mechanical and Aerospace Engineering, Cornell University.
Wu, J.-S., and Faeth, G.M. (1994), Sphere wakes at moderate reynolds numbers in a turbulent environment, *AIAA J.*, **32**(3), 535–541.